Applied Catalysis B: Environmental 180 (2016) 569–579

Contents lists available at ScienceDirect

Applied Catalysis B: Environmental

journal homepage: www.elsevier.com/locate/apcatb

Competitive HDS and HDN reactions over NiMoS/HMS-Al catalysts: Diminishing of the inhibition of HDS reaction by support modification with P

T.A. Zepeda[a,*], B. Pawelec[b], R. Obeso-Estrella[a], J.N. Díaz de León[a], S. Fuentes[a], G. Alonso-Núñez[a,c], J.L.G. Fierro[b]

[a] Centro de Nanociencias y Nanotecnología – UNAM, Km. 107 Carretera Tijuana-Ensenada, CP. 22800, Ensenada, B.C., Mexico
[b] Instituto de Catálisis y Petroleoquímica, CSIC, c/Marie Curie 2, L10, Cantoblanco, 28049 Madrid, Spain
[c] Sabbatical at the Institut de Recherches sur la Catalyse et líEnvironnement de Lyon (IRCELYON), France

ARTICLE INFO

Article history:
Received 6 April 2015
Received in revised form 12 June 2015
Accepted 8 July 2015
Available online 17 July 2015

Keywords:
Hydrodesulfurization
Dibenzothiophene
Hydrodenitrogenation
Carbazole
Mesoporous catalysts

ABSTRACT

Individual and simultaneous hydrodesulfurization (HDS) of dibenzothiophene (DBT) and hydrodenitrogenation (HDN) of carbozole reactions have been studied in the presence of hydrogen (P = 55 bar) at 310 °C in a batch reactor over a series of sulfided NiMo/P/Al-HMS catalysts modified with phosphorus (0.5–2.0 wt%). Both oxidic precursors and sulfide catalysts have been characterized by specific surface area, XRD, Raman, TPD-NH_3, HRTEM, XPS and IR spectroscopy of adsorbed pyridine. Regardless of the reaction studied, all P-containing catalysts showed higher activity than that to the P-free one. The catalyst modified with optimized amount of P (1 wt%) the best HDS activity and exhibited a lowest inhibition factor during simultaneous HDS and HDN, which was close to that of a commercial NiMo/Al_2O_3 sulfide catalyst. This was linked with formation of irregular MoS_2 structures having high concentration of brim sites as well as with its largest total acidity.

© 2015 Elsevier B.V. All rights reserved.

1. Introduction

It is well known the fact that the presence of N-containing compounds such as carbazole and quinoline has a very strong inhibitory effect on deep hydrodesulfurization (HDS) reactions because of the competitive adsorption of S- and N-containing compounds on the active sites [1–7]. However, the inhibition of the HDS reaction by competitive adsorption of N-containing compounds should be diminished by an increase of the catalyst hydrogenation ability [1–3]. In this sense, recent advances in technology for production of ultra-low sulfur transport fuels are based on a BRIM™ hydroprocessing technology developed by Topsøe et al. [8]. Indeed, the catalysts based on this technology are successfully used by many refineries because they exhibit superior hydrodesulfurization (HDS) activity and excellent stability [9,10]. The superior HDS activity of their Ni(Co)Mo phases is due to a large amount of so-called "brim sites", which are fully sulfur-coordinated sites. The brim sites, which exhibit metallic character, are involved in adsorption, C—S bond scission and hydrogenation [8]. Thus, the Ni(Co)Mo-based catalysts possessing optimized amount of those brim sites exhibited hydrogenation (HYD) functionality and enhanced rate of the direct desulfurization (DDS) reaction pathway.

Typically, the hydrotreatment reactions are catalyzed by Co(Ni)Mo(W) catalysts supported on alumina [11]. The origin of the almost exclusive use of alumina as support has been ascribed to its outstanding textural and mechanical properties and its relatively low cost [12]. However, the evidence of undesirable a very strong metal-support interaction has urged numerous studies devoted to new supports [12]. In this sense, it is known that the mesoporous silica materials, such as hexagonal mesoporous silica (HMS), exhibit a much lower metal-support interaction. Moreover, the enhancement of the catalyst hydrogenation function was observed after modification of HMS substrate with Al^{3+} ions [13]. This prompted us to study the effect of modification of the HMS substrate with both P and Al on the catalytic response of NiMo catalysts in simultaneous HDS + HDN reaction. The phosphorous was selected as second promoter because: (i), the phosphorous addition was a common practice in the preparation of commercial hydrotreating Co(Ni)Mo catalysts [14]; (ii), there are only few studies on the effect of phosphorous addition to silica-supported hydrotreating catalysts [15–18], and (iii) this effect is scarcely studied for simultaneous HDS and HDN reactions [19–23].

Besides the large body of work on the effect of support modification with phosphorous, this effect is still controversial for both

* Corresponding author.
E-mail address: trino@cnyn.unam.mx (J.L.G. Fierro).

http://dx.doi.org/10.1016/j.apcatb.2015.07.013
0926-3373/© 2015 Elsevier B.V. All rights reserved.

HDS and HDN reactions [14]. In particular, there is some confusion concerning the HDS reaction. On one hand, no detectable or negative effects of phosphorous addition were observed [16,24]. On the other hand, the positive influence was reported for the catalysts supported on alumina [10,19,20,24–26] and mesoporous silica materials [17,18]. In general, after support modification with phosphorous, the enhancement of the active phase dispersion, modification of the catalyst's acidic properties, diminishing of the metal-support interaction and changes of the properties of the Mo and Ni or Co edge sites were observed [10]. A strong interaction between phosphorous and alumina leading to formation of aluminum phosphates was reported [27].

It is well established that the effect of phosphorous depends strongly on its content being 1–1.6 wt% the most optimized one [18,27]. This is because this phosphorus content ensures the optimum composition of the polymolybdates formed and their homogeneous dispersion on the support surface [27]. In this sense, it was claimed that phosphate improved the HDN activity of $NiMoP/Al_2O_3$ sulfide catalysts by inducing the formation of the more active "NiMoS"-type II phase [28]. On the contrary, the formation of not fully sulfided "NiMoS" phase of type I was postulated for the P-free catalyst having some Mo—O—Al linkages with support [28–29]. A large amount of phosphorous species decorating support surface forced formation of "onion-type" $Mo(W)S_2$ phases, as it was confirmed by HR-TEM study of the NiMoW/SBA-16 sulfide catalysts [18], and led to decrease of the catalyst acidity [9]. Such decrease of the catalyst acidity influenced on the catalyst stability due to diminishing of coke formation [15,17].

Concerning the effect of phosphorous on the catalyst activity, it was found that the phosphorous itself does not contribute directly to the HDS reaction, but does improve the catalyst performance in HDN reaction, mainly through increasing the catalyst affinity for quinoline [29]. In this sense, it was claimed that phosphate has an influence on the overall catalyst activity only if the preceding hydrogenation reactions are not rate determining for the S- and N-elimination [28]. Interestingly, Sigurdson et al. [19] demonstrated that phosphorous doping of ternary $NiMoW/Al_2O_3$ catalysts has a stronger promotional effect for HDN than for HDS reaction. The promotional effect of phosphorus was reported also for $NiMo/Al_2O_3$ catalysts tested in HDS of gas oil spiked with 5 vol% of quinoline being the optimum P loading close to 1.0 wt% [20] whereas our previous study demonstrated that support modification with small amount of phosphorous diminishes coke formation [18].

In the present work, the effect of the support modification with P on catalytic activity and selectivity of NiMo/P/HMS-Al catalysts were examined upon testing in individual and competitive HDS + HDN reactions. The objective was to study the effect of modification of the Al-HMS support with phosphorus on the hydrogenation properties of the catalysts as well as on their resistance to deactivation by carbazole. The hexagonal mesoporous molecular sieve (HMS) was selected as support because of its high surface area, a hexagonal array of uniform mesopores, a narrow pore size distribution and thermal stability [30]. To explain the activity and selectivity results, the oxide precursors and sulfided catalysts were characterized using different techniques (N_2 adsorption–desorption, FTIR-KBr technique, laser Raman spectroscopy, X-ray diffraction (XRD), temperature-programmed sulfidation (TPS), temperature-programmed desorption of ammonia (TPD-NH_3) and FTIR spectroscopy of adsorbed NO).

2. Experimental

2.1. Preparation of supports

The Al-HMS support (Si/Al atomic ratio of 40) was prepared following a procedure similar to that described by Gontier and Tuel [31], by using dodecylamine ($C_{12}H_{25}NH_2$, Aldrich 98%) as surfactant, tetraethyl orthosilicate (TEOS 98%, Aldrich) and aluminum isopropoxide (98%, Aldrich) as silica and aluminum precursors, respectively. The reaction mixture was slightly modified by the addition of the swelling agent mesitylene (C_9H_{12}, Aldrich 98%), as first proposed by Kresge et al. [32]. The material obtained was dried at room temperature for 16 h and then at 110 °C for 2 h, and finally calcined in air at 500 °C for 4.5 h, reaching this temperature in 3.5 h. The P/HMS-Al materials were prepared by functionalization of HMS-Al substrate with $-PO_3H_2$ groups following the procedure described by Kawi et al. [33]. Briefly, the substrate grafting with $-PO_3H_2$ groups was performed by impregnation of substrate (pore filling method) with an aqueous solutions of H_3PO_4 (Fluka; 85 wt% in water) having appropriate concentrations to obtain substrates with phosphorus loadings of 0.5, 1.0, 1.5 and 2.0 wt%. As the HMS-Al substrate possesses extraframework Al atoms, its point of zero charge (PZC) was found somewhat higher than that of silica (3.5). Thus, for the deposition of the negatively charged $[PO_4]^{3-}$ ions on the negatively charged surface of HMS-Al, the pH of aqueous solution of H_3PO_4 was adjusted to about 2.5. Subsequently, the resulted solids were dried at room temperature for 16 h and then at 110 °C for 2 h, and finally calcined at 500 °C for 4.5 h in static air reaching this temperature within 3.5 h. The supports will be coded hereafter as (*x*)P/HMS-Al, where *x* is wt% of P.

2.2. Preparation of oxide precursors

In this work, all NiMo catalysts were prepared by simultaneous impregnation of the synthesized (*x*)P/HMS-Al solids (pore filling method) with aqueous solutions of ammonium heptamolybdate ($(NH_4)_6Mo_7O_{24}{\cdot}4H_2O$; Aldrich 99%) and nickel nitrate [$Ni(NO_3)_2{\cdot}6H_2O$, Aldrich 98%]. The nominal molybdenum and nickel contents were 9.0 and 3.2 wt%, respectively. Ammonia was added in order to shift the polymolybdate ↔ monomolybdate equilibrium [34]. The obtained solids were dried at room temperature for 18 h, and then at 110 °C for 2 h, and calcined for 4.5 h at 500 °C reaching this temperature within 3.5 h. The NiMo/(*x*)P/HMS-Al catalysts will be coded hereafter as Cat-P(*x*), where *x* is wt% of P.

2.3. Characterization of supports, oxide precursors and sulfided catalysts

The X-ray patterns of the supports, oxide precursors and fresh sulfided samples were recorded on a Rigaku 2100 diffractometer, using monochromatic Cu Kα radiation (λ = 0.1541 nm). The diffractograms were recorded in the 2θ range of 0.15–80° at a step of 0.02°.

The textural properties of the sulfided catalysts were determined by N_2 adsorption-desorption isotherms at −196 °C with an ASAP 2000 Micromeritics equipment. Prior to analysis, the oxide precursors were sulfided *ex-situ* in a U-shape glass reactor under the same conditions as described in the section on catalytic activity tests. After sulfidation, the samples were cooled to room temperature under N_2 flow and transferred into the Micromeritics apparatus in an Ar atmosphere without exposing the sample to air. Prior to the experiments, the samples were degassed at 270 °C in a vacuum for 5 h. The volume of adsorbed N_2 was normalized to standard temperature and pressure. Specific surface area (S_{BET}) was calculated by the BET equation applied to the range of relative pressures $0.05 < P/P_0 < 0.30$. Average pore diameter was calculated by applying the Barret–Joyner–Halenda method (BJH) to the adsorption branches of the N_2 isotherms. The cumulative pore volume was obtained from the isotherms at $P/P_0 = 0.99$.

The acidity of fresh sulfided samples was studied by in situ infrared (IR) spectroscopy of adsorbed pyridine using a Agilent 660 FTIR spectrophotometer working at a resolution of 4 cm^{-1}.

Table 1
Textural[a] properties of the NiMo/P(*x*)/HMS-Al sulfided catalysts.

Samples	S_{BET} (m^2/g)	d_p (nm)	V_p (cm^3/g)	Concentration of Brønsted and Lewis acid sites[b]			
				Brønsted ($\mu mol\ g_{cat}^{-1}$)	Lewis ($\mu mol\ g_{cat}^{-1}$)	Total acidity ($\mu mol\ g_{cat}^{-1}$)	Brønsted/Lewis ratio
Cat-P0.0	733	2.9	0.97	0.31	1.21	1.52	0.26
Cat-P0.5	728	3.0	0.92	0.45	1.56	2.01	0.29
Cat-P1.0	712	3.1	0.88	0.80	1.69	2.49	0.47
Cat-P1.5	658	2.9	0.81	0.54	1.59	2.13	0.34
Cat-P2.0	527	2.4	0.66	0.40	1.55	1.95	0.26

[a] As determined from N_2 adsorption–desorption isotherms at −196 °C. S_{BET}: specific BET surface area; d_p: average pore diameter; V_p: total pore volume.
[b] As determined by FT-IR spectroscopy of adsorbed pyridine. The amounts of the Brønsted acid and Lewis acid sites were estimated from the integrated absorbance of both bands using the integrated molar extinction coefficients reported by Emeis [35].

The reactor system consists of an in situ DRIFTS reactor (praying mantis) and a Harrick diffuse reflectance low temperature cell (HVC-DRP cell), which are situated inside an IR bench. The samples were sulfided in situ with a 15% H_2S/H_2 mixture at 623 K for 1 h, and then outgassed under 10–5 mbar during 1 h. Following the pre-treatment, the reactor was cooled slowly back to 373 K and the sample was outgassed under 10^{-5} mbar during 1 h. Then, the sample was exposed to a gaseous flow of pyridine (partial pressure ≈5 mbar) for 40 min. Physisorbed pyridine was removed from the catalyst surface by vacuum outgassing at 10^{-5} Torr, at 393 K for 0.5 h. Then, the final IR spectra of chemisorbed pyridine were collected to characterize the acid surface.

HRTEM micrographs were collected on a JEOL-2010F instrument. The samples were suspended in heptane as solvent in order to be deposited on lacey carbon (440 Mesh) Cu grid holders.

The X-ray photoelectron spectra of the freshly sulfided catalysts were recorded using a VG Escalab 200R spectrometer equipped with a hemispherical electron analyzer and a Mg Kα ($h\nu$ = 1253.6 eV) X-ray source. In order to protect the samples from the contact with air, they were kept in *i*-octane until being transferred into the XPS apparatus. The samples were first placed in a stainless steel holder mounted on a sample-rod in the pretreatment chamber of the spectrometer and then degassed at 150 °C for 1 h before transfer to the analysis chamber. Charge effects were corrected by taking the binding energies (BE) of the C 1s peak of adventitious carbon at 284.9 eV. Analyses of the peaks were performed with the software provided by VG and using non-linear least squares fitting program.

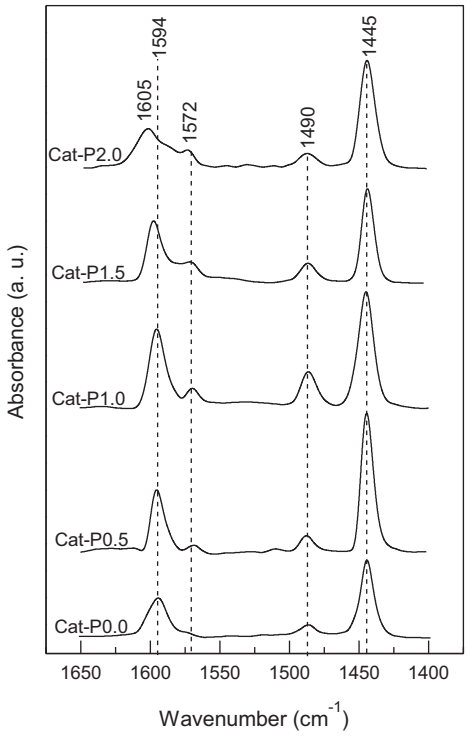

Fig. 1. DRIFT spectra of adsorbed pyridine for NiMo/P(*x*)/HMS-Al sulfide catalysts.

2.4. Catalytic activity measurements

The catalyst activity was evaluated in the individual and simultaneous hydrodesulfurization (HDS) of dibenzothiophene (DBT) and hydrodenitrogenation (HDN) of carbazole reactions carried out in a batch Parr reactor at the same experimental conditions (T = 320 °C and total hydrogen pressure of 55 bar). Prior to the experiment, the catalyst was sulfided ex-situ with a H_2/H_2S gas mixture (10 vol% H_2S; a flow of 60 mL min^{-1}) from 150 °C up to 400 °C (heating rate of 4 °C min^{-1}) and kept this temperature for 2 h. After purging with inert gas to eliminate H_2S, the sample was transferred to the reactor in an argon atmosphere with the aim to avoid contact with air. Depending on the reaction, the reactor was charged with 0.2 g of the sulfided catalyst (particle size between −80/+100 mesh) and 100 mL of the following feeds:

(i) *HDS of DBT*. Feed composition was DBT (550 ppm of S) dissolved in 100 mL of *n*-hexadecane.
(ii) *HDN of carbazole*. Feed composition was: carbazole (180 ppm of N) dissolved in 100 mL of hexadecane/*p*-xylene solvent's mixture (90/10% v/v). This solvent mixture was employed in order to assess the total solubility of carbazole.
(iii) Hydrodesulfurization of dibenzothiophene in presence of carbazole. Feed composition: DBT (550 ppm of S) and carbazole (0, 50, 100 and 180 ppm of N) dissolved in 100 mL of hexadecane/*p*-xylene solvent's mixture (90/10% v/v).

For each reaction, the reactions products were analyzed by GC on a PerkinElmer XL equipment using 30 m capillary column coated with a non-polar methyl silicone phase (DB-1, J & W). A commercial $NiMo/Al_2O_3$ catalyst (Mo = 12 wt%, Ni = 4.0 wt%, P = 2.4 wt%) was used as reference.

3. Results and discussion

3.1. Catalyst characterization

After sulfidation, the surface areas of catalysts varied in the range of 527–733 $m^2\ g^{-1}$ (Table 1). A decrease in both surface area and pore volume was observed when P was introduced into the support with respect to the P-free sample. This decrease was almost insignificant for the Cat-P0.5 and Cat-P1.0 samples (<3%) and a much larger for Cat-P1.5 and Cat-P2.0 catalysts (11.4 and 39.1%, respectively) with respect to P-free sample. Similarly to the S_{BET}, a slight increase is observed for average pore diameter by increasing

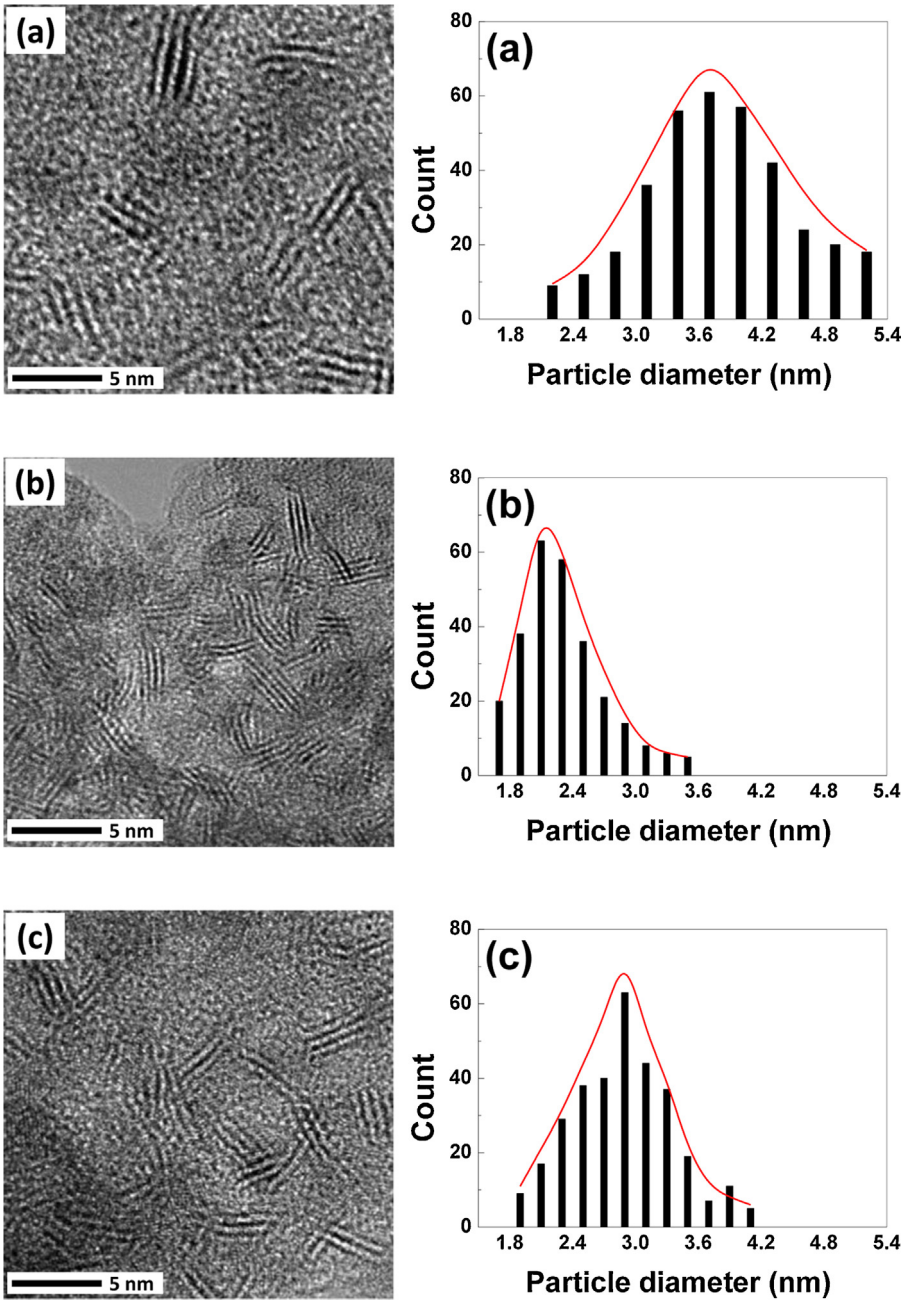

Fig. 2. HRTEM images of MoS_2 sheets observed on Cat-P0.0 (a), Cat-P1.0 (b) and Cat-P2.0 (c) sulfide catalysts.

the P content in the materials up to 1%. Noticeably, the catalyst with a largest P content (2.0 wt%), showed a small decrease of its average pore diameter with respect to P-free one (from 2.9 to 2.4 nm) suggesting that its micropores were blocked by P species. The large decrease in the surface area, pore diameter and pore volume at high P-loadings suggests the formation of large MoS_2 particles partially blocking support structure, in agreement with previous published reports [13,18].

3.1.1. *DRIFT spectroscopy of adsorbed pyridine*

The acidity of fresh sulfide samples was studied using in situ DRIFT study of adsorbed pyridine (Fig. 1). The corresponding amount of each acid site-type, Lewis and Brønsted are reported in Table 1. The acidity amount was calculated from FT-IR spectra, quantitative analysis was done as reported in [35]. The samples showed similar spectra in the range 1400–1650 cm^{-1}. The bands assigned to the pyridine chemisorbed on Lewis sites and hydrogen-bonded pyridine is observed at 1445 and 1594–1605 cm^{-1}, respectively [36]. The band located at 1572 cm^{-1} is assigned to the vibration mode of pyridine ion adsorbed on Brønsted sites, while a band observed at 1490 cm^{-1} is assigned to pyridine associated with both Lewis and Brønsted sites [37]. The influence of P on the both types of acid sites could be obtained by analyzing the Brønsted/Lewis acidity ratio. Table 1 recompiled the Brønsted sites concentration calculated by applying to the absorbance of the band at 1545 cm^{-1} the molar extinction coefficient of this band determined by Emeis [35]. The amounts of the Brønsted acid and Lewis acid sites were estimated from the integrated absorbance of both bands using the integrated molar extinction coefficients (1.67 cm μmol^{-1} for the 1548 cm^{-1} band and 2.22 cm μmol^{-1} for the 1450 cm^{-1} band) reported in the literature [35]. As seen in Table 1, the total acidity and Brønsted/Lewis acidity

ratio follows the same trends: Cat-P1.0 > Cat-P1.5 > Cat-P0.5 > Cat-P2.0 = Cat-P0.0. Thus, all P-containing samples show higher acidity in the comparison with the P-free sample. The Cat-P1.0 sample exhibit largest total acidity and Brønsted acidity among the catalysts studied. Taking into account that sulfidation led to an increase of support acidity by attaching —SH groups on the support surface, the IR-py study of the sulfided catalysts gave information on the acidity of both support and metal sulfides.

3.1.2. HRTEM

To evaluate the influence of P on the active phase dispersion, structure and nature of the active sites, the fresh sulfide catalysts were studied by HRTEM microscopy. In Fig. 2 are compared high magnification images of MoS_2 sheets observed on P-free and two most representative P-containing catalysts (Cat-P1.0 and Cat-P2.0) together with statistical evaluation of about 250 particles from various HRTEM images. As expected, all spent catalysts present the typical fringes of Mo(W)S_2 crystallites as well. The average MoS_2 particle size deduced from slabs length was found to follow the trend: Cat-P0.0 (3.8 nm) > Cat-P2.0 (2.9 nm) > Cat-P1.0 (2.2 nm). Thus, the Cat-P1.0 with optimized P loading exhibits the best MoS_2 dispersion. Moreover, it was found that the support modification with P did not influence on the number of stacking layers showing all catalysts a highly stacked layers of Mo(W)S_2 particles (3 ± 1 layers). The Cat-P0.0, Cat-P1.0 and Cat-P2.0 catalysts exhibited the average number of stacking layers of 3.5, 3.1 and 3.3, respectively.

3.1.3. FTIR spectroscopy of adsorbed NO

It is commonly accepted that the NO probe molecule could be selectively adsorbed to the edge or the corner sites of MoS_2-like structures or to nickel atoms at the edges of MoS_2 in NiMoS catalysts [38]. Fig. 3 presents the FT-IR spectra of adsorbed NO. As seen in this figure, all catalysts presented two major bands around 1867 and at 1795 cm^{-1} together with a broad band located around 1640 cm^{-1}. Based on previous studies on sulfided CoMo and NiMo catalysts [2,38–41], the broad bands with maxima at about 1867 and 1795 cm^{-1} contain two contributions from NO adsorbed on non-sulfided Ni^{2+} and sulfided Ni^{2+} sites indicating a partial sulfidation of Ni promoter species upon the sulfidation conditions employed. The broad peak observed at lower wavenumbers could be assigned to the asymmetric stretching vibrations of NO adsorbed on $Mo^{\delta+}$ sulfided species. Generally, regardless of P content in the sulfided catalysts, no significant shift in position of those IR bands was observed with respect to P-free sample. The Cat-P1.0 sample shows a largest area of the band corresponding to the sulfided $Mo^{\delta+}$ species among the catalysts studied suggesting a better dispersion of its MoS_2 phase. With an increase of the P content from 1.0 to 1.5 and 2.0 wt%, the area of the broad band observed at 1640 cm^{-1} decreased suggesting that a further increase in the content of P has a negative effect on the dispersion and the sulfiding properties of Mo species.

In the case of the Ni bands results presented here showed no clear evidence regarding the effect of P on the amount of Ni interacting with Mo in the active phases. In general, the total area of broad band with maximum at 1867 cm^{-1} increased after P loading to the catalysts but this increase is not linear. Thus, both Cat-P0.5 and Cat-P1.5 samples show lower area of this band as compared to the Cat-P1.0 and Cat-P2.0 counterparts (Fig. 3). From these results it can be concluded that: (i), the presence of P on the catalyst surface influenced the dispersion of the MoS_2 active phase, led to increase of the interaction of Ni promoter with Mo species, and it affected the sulfidation degree of Ni species to a different extent depending on the amount of P present in the substrate.

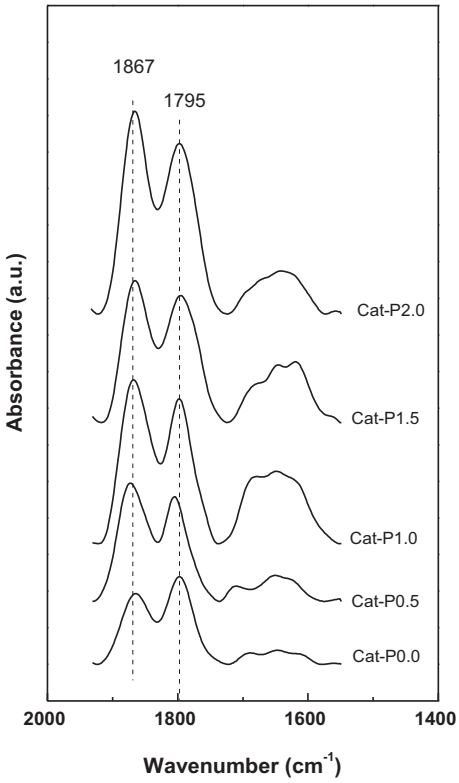

Fig. 3. Comparison of FT-IR spectra of NO adsorbed on NiMo/P(x)/HMS-Al sulfide catalysts: (a) Cat-P0.0; (b) Cat-P0.5; (c) Cat-P1.0; (d) Cat-P1.5; (e) Cat-P2.0.

Table 2
Binding energy of core electrons of freshly sulfided catalysts from XPS[a].

Catalyst	Mo $3d_{5/2}$		Ni $2p_{3/2}$		P 2p
	MoS_2	Mo^{6+}	Ni—S	NiO	
Cat-P0.0	228.9 (71)	231.4 (29)	852.4 (39)	855.3 (61)	–
Cat–P0.5	228.9 (74)	231.2 (26)	852.5 (40)	855.3 (60)	134.9
Cat-P1.0	228.9 (67)	231.3 (33)	852.3 (36)	855.2 (64)	135.0
Cat-P1.5	228.9 (79)	231.1 (21)	852.5 (48)	855.3 (52)	134.8
Cat-P2.0	229.0 (78)	231.2 (22)	852.3 (45)	855.3 (55)	134.7

[a] The percentage of each species is given in parenthesis.

3.1.4. X-ray photoelectron spectroscopy (XPS)

To gain further insight into the chemical composition and distribution of the different elements on the catalysts surface, the freshly sulfided catalysts were studied by X-ray photoelectron spectroscopy. Our objective was to evaluate the effect of P loading on the type of species formed and their surface exposure for NiMoS/P/HMS-Al catalysts. For all catalysts, the S 2p peak binding energy at 161.2 ± 0.1 eV was characteristic of S^{2-} ions. The BE values of the Mo $3d_{5/2}$, Ni $2p_{3/2}$ and P 2p core-levels are compiled in Table 2. The values in parentheses correspond to the percentage of sulfided or unsulfided Mo and Ni species. An example of the decomposition of Mo 3d and Ni $2p_{3/2}$ spectra is shown in Fig. 4. As seen in this figure, the XPS spectra of the Ni 2p emission line show shake-up satellite lines. Since the line-shape of the Ni $2p_{3/2}$ peak, and especially its satellite, was unsymmetrical and broad, we applied an empirical method to roughly fit the curve using Gaussian/Lorentzian distributions. For all samples, the Ni $2p_{3/2}$ main binding energies are observed at about 852.4 eV and 855.3 eV suggesting that Ni^{2+} is present on the catalyst surface as Ni—S (probably Ni_3S_2) and Ni—O oxides, respectively, according to previous reports [42–43]. From the areas of sulfided and oxidic nickel species it is evident that Cat-P1.5 and Cat-P2.0 catalysts show, in agreement with

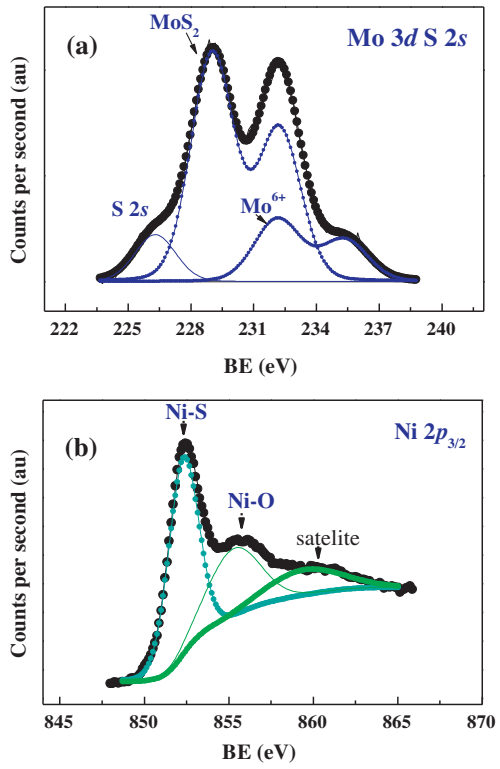

Fig. 4. Mo 3d S 2s (a) and Ni $2p_{3/2}$ (b) core level spectra of sulfided Cat-P2.0 catalyst.

the FTIR spectra of NO (cf. Fig. 3), a largest proportion of sulfided Ni species among the catalysts studied.

For the Mo 3d core-level spectra, curve fitting procedure revealed the presence of two Mo 3d doublets: a major one with the BE values at 228.9 eV fits well with that expected for MoS_2 species, and a minor one about 231.2 eV ascribed to unsulfided (Mo—O) and/or partially sulfided (O—Mo—S) species probably located at the support interface [42–43]. Whatever the P-loading, no significant differences in the BE of Mo 3d can be noted for all catalysts studied. The exception is a larger sulfidation degree of Mo and Ni species on the Cat-P1.5 and Cat-P2.0 (Table 2) suggesting a decrease of the metal-support interaction induced by presence of a large amount of phosphate species on the support surface [28]. Contrary to the XPS study of Raybaud and c0-workers **[**42–43], the formation of "Ni—Mo—S" phase at low temperature employed for the catalyst sulfidation (400 °C) is hardly possible. Because the low temperature employed for catalyst sulfidation (400 °C), the percentage sulfidation was not so high (Mo = 67–79% and Ni = 36–48%), as confirmed by IR NO adsorption and XPS studies. Moreover, since the samples were ex situ sulfided, one might expect some oxidation during sample handling. Besides this, the XPS measurements of the samples ex situ sulfide could be more realistic than in-situ because the ex-situ sulfidation with a H_2S/H_2 mixture prevents the samples from coking during the sulfidation step [43].

The quantitative XPS analyses data are shown in Table 3. Considering the surface exposure of the molybdenum and nickel species, as deduced from Mo/Si and Ni/Si atomic ratio calculated from the peak intensities of the elements, two observations are made: (i) regardless of the P-loading, all catalysts show similar Ni and Mo surface exposures; and (ii), two catalysts with a the largest P loadings (1.5 and 2.0 wt%) show a larger sulfidation degree than the other samples, as deduced from the S/(Mo + Ni) atomic ratio. Taking into account that the surface exposure of nickel sulfide species is similar for all catalysts studied, this means that support grafting with P promote sulfidation of Mo species only. As a consequence, both latter samples show a largest MoS_2 species surface exposure among the catalysts studied. In addition, the surface exposure of Al species is high for all catalysts studied.

Table 3
Surface atomic ratios of freshly sulfided catalysts.

Catalyst	Mo/Si	Ni/Si	(Mo + Ni)/Si	S/(Mo + Ni)	P/Si	Al/Si
Cat-P0.0	0.021	0.011	0.032	1.43	–	0.021
Cat–P0.5	0.020	0.009	0.029	1.45	0.005	0.023
Cat-P1.0	0.023	0.012	0.035	1.41	0.009	0.020
Cat-P1.5	0.027	0.010	0.037	1.53	0.015	0.024
Cat-P2.0	0.024	0.009	0.033	1.50	0.017	0.022

Table 4
Selectivity in individual HDS of DBT[a] for NiMo/P(x)/HMS-Al and $NiMo/Al_2O_3$ (reference) sulfide catalysts.

Catalyst	Selectivity[b] (%)				HYD/DDS[c]
	BP	CHB	DCH	THDBT	
Cat-P0.0	91.3	3.9	2.3	2.5	0.10
Cat–P0.5	86.1	6.9	4.8	2.2	0.16
Cat-P1.0	77.9	12.2	6.9	3.0	0.28
Cat-P1.5	83.7	7.8	6.1	2.4	0.20
Cat-P2.0	86.0	5.6	4.7	3.7	0.16
$NiMo/Al_2O_3$	84.1	8.2	5.5	2.2	0.19

[a] The reaction conditions were: T = 320 °C; P = 55 bar; batch reactor.
[b] Selectivity at 30% conversion: BP: biphenyl; THDBT: tetrahydrodibenzothiophene; CHB: cyclohexylbenzene; DCH: dicyclohexyl.
[c] Direct desulfurization is denoted as DDS, hydrogenation pathway is denoted as HYD. The HYD/DDS ratio is calculated from selectivity of the products [(CHB + DCH + THDBT)/BP].

3.2. Catalytic activity

The synthesized catalysts were evaluated in the HDS of DBT reaction in a batch reactor at 320 °C and under total hydrogen pressure of 55 bar. A conventional $NiMo/Al_2O_3$ catalyst was used as reference. The initial reaction rates for the HDS of DBT as a function of P/Si atomic ratio (from XPS) are shown in Fig. 5(a). All catalysts modified with P exhibited higher activities than the P-free and the reference $NiMo/Al_2O_3$ catalysts. However, the initial catalyst activity follows volcano curve trend. The maximum increase in the catalytic activity is observed up to P content of 1.0 wt%. This sample was 50 and 67% more active in comparison with the P-free and reference samples, respectively.

Table 4 shows the selectivity achieved at DBT conversion of 30% and HYD/DDS ratios for the different catalysts. Regardless of the P-loading, the reaction products were: biphenyl (main product), tetrahydrodibenzothiophene (traces), cyclohexylbenzene and dicyclohexyl. The preferential formation of biphenyl (selectivity about 80%) indicates that the DDS route of DBT transformation was favoured with respect to HYD one. This is in good agreement with previous reports on the Ni-promoted catalysts [44]. Scheme 1(a) shows the reaction network of DBT HDS which includes two reaction pathways: hydrogenation (HYD) and direct desulfurization (DDS) [45–46]. In the hydrogenation (HYD) route of this reaction, the DBT is hydrogenated in a first step to produce tetrahydrodibenzothiophene (TH-DBT) and then the sulfur is eliminated from this intermediary product leading to formation of cyclohexyl benzene (CHB), which is further hydrogenated to produce dicyclohexyl (DCH). During direct desulfurization (DDS) route of HDS of DBT reaction, the C—S bond cleavage occurs by hydrogenolysis leading to formation of biphenyl (BP). Considering the selectivity data, this is a main reaction product for all catalysts studied. To obtain information about the effect of phosphorus for the preferential route of the HDS reaction, the HYD/DDS ratio was calculated considering the selectivity data compiled in Table 4. Data indicate that regardless

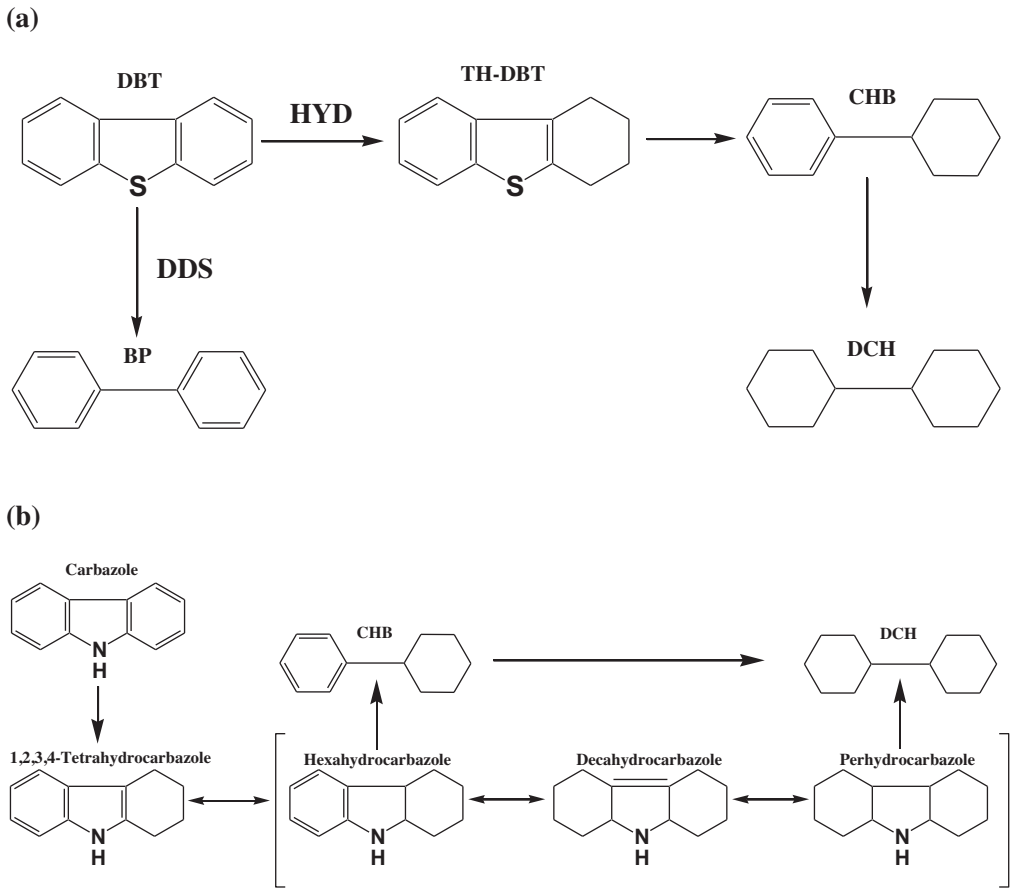

Scheme 1. Reaction schemes for the hydrodesulfurization of DBT (a) and hydrodenitrogenation of carbazole (from [10]) (b).

of P-loading, the HYD/DDS ratio is always lower than 1. Nonetheless, the incorporation of P onto HMS support favors the HYD route of DBT transformation. Thus, taking into account that HYD route of HDS of DBT occurs via flat mode of DBT adsorption through π-complexation of the aromatic ring [46], we might to conclude that P-containing catalysts did not show steric hindrance for DBT adsorption. On the contrary, it is commonly assumed that the vertical mode of DBT adsorption leads to the formation of biphenyl. Since the P-free sample showed largest biphenyl formation among the catalysts studied (Table 4), this may indicate the preferential vertical mode of DBT adsorption on the active phases of this sample. The enhancement of the specific activity on the Cat-P1.0 might to suggest the creation of new HYD sites. The so-called brim sites of MoS_2 phase are probably play a role in the HYD pathways of DBT transformation [8]. Thus, for the individual HDS of DBT reaction, an increase of HYD/DDS selectivity ratio with an increase of P loading might suggest the presence of MoS_2 phase having a large amount of those sites. However, this should be a subject of future research.

3.2.1. HDN of carbazole

Before evaluating the effect of carbazole on the HDS of DBT, HDN experiments of pure carbazole were conducted under similar reaction conditions as those for the HDS of DBT although a 70/30 wt% of *n*-hexadecane/*p*-xylene was used as solvent to allow perfect solubilization of carbazole. Fig. 5(b) shows the influence of P species surface exposure (XPS) on the initial reaction rates in the HDN of carbazole (180 ppm N). As expected, the comparison of the activities in HDS and HDN reactions clearly indicated a larger catalyst activity in the former reaction than in the latter. Similarly to HDS of DBT, all catalysts modified with P exhibited higher activities in the HDN of carbazole than the P-free. This trend is similar to that observed for the HDS of DBT. Nevertheless, only the Cat-P1.0 and Cat-P1.5 catalysts were more active than the $NiMo/Al_2O_3$ reference catalyst.

Table 5
Activity and selectivity in individual HDN of carbazole[a] over NiMo/P(x)/HMS-Al catalysts.

Catalyst	Rate × 10^8 ($mole_{Cabazole}$ g^{-1} s^{-1})	Selectivity[b](%)		
		CHB	DCH	THC
Cat-P0.0	11	91	7	2
Cat–P0.5	17	85	11	4
Cat-P1.0	43	74	17	9
Cat-P1.5	32	82	14	4
Cat-P2.0	20	86	10	4
$NiMo/Al_2O_3$	36	74	21	5

[a] The reaction conditions were: $T = 320\,^{\circ}C$; $P = 55$ bar. The nitrogen concentration was 180 ppm in 90/10 wt% mixture of *n*-hexadecane/*p*-xylene.
[b] Selectivity at 30% conversion: THC: tetrahydrocarbazole; CHB: cyclohexylbenzene; DCH: dicyclohexyl.

Table 5 summarizes the selectivity for the HDN of carbazole obtained at 30% of conversion. The major products observed were cyclohexylbenzene (CHB) and dicyclohexyl (DCH) whereas 1,2,3,4-tetrahydrocarbazole (THC) was present only in small amounts, except for the 1.0% catalyst showing a relatively large yield of this latter product. It is well known that HDN does not occur by direct denitrogenation [1–7]. Indeed, as biphenyl was not formed, it indicates that direct elimination of NH_3 did not occur and all those products were obtained by successive hydrogenation of different —C=C— bonds of the aromatics rings of carbazole. Thus, considering the products detected, the reaction mechanism over our catalysts might follow the reaction network shown in Scheme 1(b), as it was

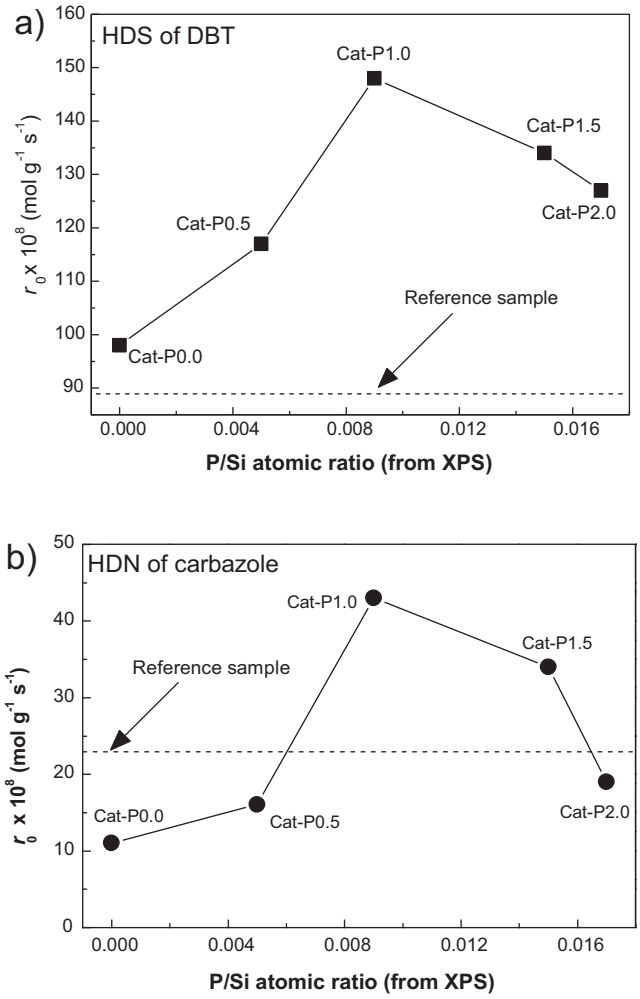

Fig. 5. Influence of P surface exposure (from XPS) on the initial reaction rates for the HDS of DBT (a) and the HDN of carbazole (180 ppm of N) (b) (batch reactor, T = 320 °C; P_{H2} = 55 bar).

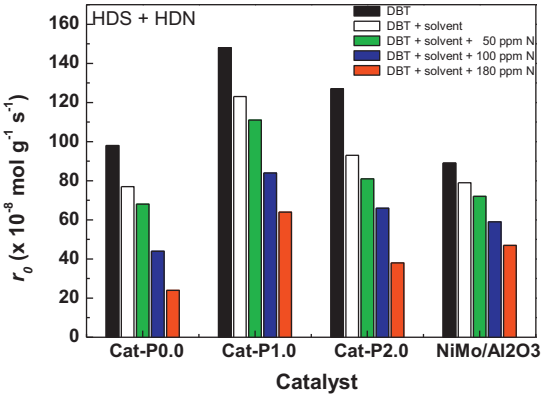

Fig. 6. Inhibition effect of solvent (90/10 %/% of *n*-hexadecane/*p*-xylene) (a) and carbazole concentration (50, 100 and 180 ppm of N) during DBT transformation over NiMo/P(*x*)/HMS-Al and a reference NiMo/Al_2O_3 sulfide catalysts (batch reactor, T = 320 °C; P_{H2} = 55 bar).

proposed by Nagai et al. [5]. In this reaction scheme carbazole is firstly hydrogenated to produce 1,2,3,4-tetrahydrocarbazole (THC), a second reaction step involves the successive hydrogenation of THC to produce hexahydrocarbazole (HHC), decahydrocarbazole (DHC) and perhydrocarbazole (PHC). Elimination of NH_3 from hexahydrocarbazole and perhydrocarbazole led to formation of cyclohexylbenzene (CHB) and dicyclohexyl (DCH), respectively. Direct hydrogenation of cyclohexylbenzene to dicyclohexyl, as it was proposed for the HDS of DBT in Scheme 1(a), cannot be precluded. The intermediate HHC, DHC and PHC products were not detected indicating that they were quickly transformed into CHB and DCH.

3.2.2. *Effects of solvent and carbazole on the DBT HDS*

For the feedstock containing pure DBT, the catalyst HDS activity follows the trend: Cat-P1.0 > Cat-P2.0 > Cat-P0.0 > NiMo/Al_2O_3 (Fig. 6). Thus, in the absence of solvent, the P-free catalyst showed a higher HDS activity than NiMo/Al_2O_3 reference catalyst being the most active catalyst modified with 1 wt% of P. To see if we could improve the catalyst activity we conducted the DBT HDS test by using a mixture of DBT and solvent (*n*-hexadecane and *p*-xylene (90/10 %/%). Fig. 6 illustrates the effect of solvent for the DBT transformation over different catalysts including reference NiMo/Al_2O_3 sample. As seen in this figure, all catalysts exhibited a lower HDS activity when reaction was performed in the presence of solvent. This retarding effect of the solvent could be explained considering the competitive adsorption of DBT and the solvent molecules [2,47–49]. Taking into account that the solvent composition was 90% of *n*-hexadecane and only 10% of *p*-xylene, the inhibition of HDS reaction should be mainly due to *n*-hexadecane. Besides this, some inhibition by competitive *p*-xylene adsorption on the active sites cannot be excluded.

In order to gain insight of the effect of nitrogen-containing species on the DBT HDS, the HDS reaction was carried out simultaneously with the HDN of carbazole. Regardless the catalyst tested, when carbazole was added to the feedstock containing both DBT and solvent (*n*-hexadecane and *p*-xylene), a decrease in the HDS activity was observed with respect to individual HDS reaction carried out at the same conditions (Fig. 6). The effect of carbazole concentration in the HDS of DBT over different catalysts was evaluated using different N concentrations (50, 100 and 180 ppm of N). As expected, an increase in N concentration led to decrease of DBT HDS (Fig. 6). The effect of the support can be observed if the P-free and the reference catalysts are compared (Fig. 6). At a highest carbazole concentration (180 ppm of N), the HDS activity follows trend: Cat-P1.0 » reference > Cat-P2.0 > Ca-P0.0. Thus, the inhibiting effect of carbazole on the HDS of DBT was more pronounced in the P-free catalyst than in the reference one, particularly when 180 ppm of N was added to the feed mixture. To evaluate and compare the degree of inhibition of carbazole in the HDS of DBT an inhibition factor was defined as follows [50]:

$$\theta = \frac{(r_{DBT}) - (r^{N}_{DBT})}{(r_{DBT})} \quad (1)$$

The inhibiting factor against carbazole concentration is shown in Fig. 7. At low nitrogen concentrations the inhibiting effect of carbazole on the HDS of DBT was more or less the same for all catalysts. At 100 ppm of nitrogen the inhibiting effect of the Cat-P1.0 and Cat-P2.0 catalysts was very similar, on the other hand the P-free catalyst exhibited the highest inhibiting factor whereas the reference catalyst was the less affected. Finally, when nitrogen concentration was increased to 180 ppm the Cat-P0.0 and the Cat-P2.0 catalysts were considerably more affected than the Cat-P1.0 catalyst which exhibited a better resistance to the presence of carbazole but still was slightly more affected than the reference one.

The HYD/DDS selectivity ratio of a mixed feed containing different carbazole concentrations are compiled in Table 6 and Fig. 8 whereas those of individual HDS reaction are listed in Table 4. As seen in Table 6, regardless of the feed used (individual or mixed), all P-containing catalysts exhibited a larger HYD/DDS ratio than their P-free counterpart. Moreover, for all catalysts a decrease of the

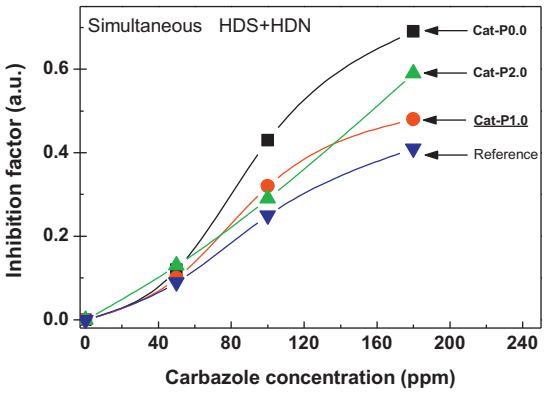

Fig. 7. Influence of carbazole concentration on the inhibition factor in simultaneous HDS + HDN reactions over NiMo/P(x)/HMS-Al sulfide catalysts (batch reactor, T = 320 °C; P_{H2} = 55 bar).

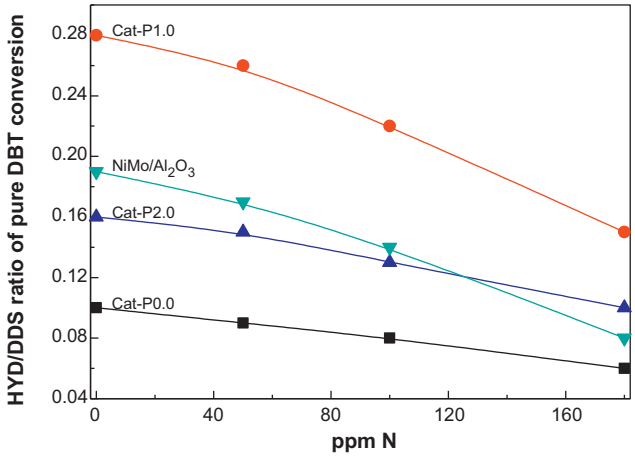

Fig. 8. Inhibition effect of solvent (90/10 %/% of n-hexadecane/p-xylene) and carbazole concentration (50, 100 and 180 ppm of N) on HYD/DDS selectivity's ratio during DBT transformation over NiMo/P(x)/HMS-Al and a reference $NiMo/Al_2O_3$ sulfide catalysts (batch reactor, T = 320 °C; P_{H2} = 55 bar).

HYD/DDS ratio was observed with an increase of carbazole concentration, in agreement with study by Topsøe et al. [8]. The most active Cat-P1.0 catalyst exhibits also the best hydrogenation activity, as confirmed by its largest HYD/DDS ratio (Table 6). Thus, one may conclude that support modification with optimized amount of P diminished the inhibition of HDS reaction of carbazole. Considering the kinetic characterization of hydrogenation and hydrogenolysis sites of sulfided $CoMo/Al_2O_3$-SiO_2 catalysts by Ho and Qiao [3] we could assume that an increase of temperature could mitigate the inhibition effect of carbazole on the HDS reaction. This should be a subject of our future research.

3.3. Catalyst activity-structure correlation

In this work, the HMS-Al substrate was impregnated with aqueous solution of H_3PO_4 at pH 2.5, which is below the isoelectric point of this material (PZC ≈ 3.5). At such conditions, the PO_4^- anions became attached to the —OH groups of support. Taking into account the relatively low P-loading of all catalysts studied, the reaction of single surface hydroxyl groups might be predominant during its support preparation, as it is visualized in Scheme 2. Upon calcination, not only P—OH groups are formed but also bulk P_2O_5 moieties decorating the support surface, as derived from an increase of acidity (from TPD–NH_3) and XPS measurements, respectively. Then, the presence of P_2O_5 modifies the distribution of OH groups on the

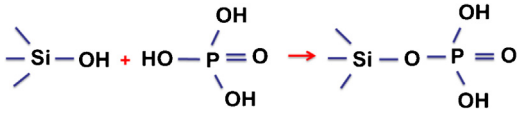

Scheme 2. Formation of —PO_3H_2 groups by single bonding of H_3PO_4 with —OH groups of Al-HMS substrate.

substrate and affects the distribution and type of Mo species [51]. Consequently the dispersion and structure of Mo species is a consequence of the modification of the substrate's isoelectric point and a change in the interaction of the adsorption of molybdate species during the impregnation procedure. The presence of a P_2O_5 phase in sulfided samples was confirmed by XPS. Considering the high specific area of the catalysts and information provided by XPS, it is likely that P_2O_5 nanoparticles could be located on the support surface rather than on the metal sulfides.

Before activity tests, the samples were sulfided at 400 °C with a H_2S/H_2 mixture. XPS study of the fresh sulfided catalysts indicated that at this temperature MoO_3 was converted to MoS_2 whereas phosphorous oxides remain intact, in agreement with Teng et al. [52]. Temperature higher than 600 °C is required for converting MoS_2 into MoP in the presence of H_2 and volatile phosphorous by reaction [52]:

$$MoS_2(s) + PO_x(s) + (x+2)H_2(g) \rightarrow MoP(s) + xH_2O(g) + 2H_2S(g)$$

To confirm that that MoP and/or Ni_2P phases cannot be formed along testing, the sulfided Cat-P2.0 sample was subjected to H_2-pretreatment at temperature higher than those used for activity test (400 °C vs. 320 °C). Then, XRD pattern of the H_2-treated Cat-P2.0 sulfide sample was recorded. In the Fig. 4 in SI (Supplementary information), the XRD profile did not exhibit any crystal structure of MoP and/or Ni_2P phases. Thus, the formation of MoP phase at reaction conditions employed can be precluded.

With exception of the Cat-P2.0, the pore size of the sulfide catalysts is about 3.0 nm in diameter, which may be large enough for three-ring compounds like DBT. The difference in the performance of the P-free and P-containing catalysts in simultaneous HDS and HDN may be due to reasons: one is the difference in metal surface exposure (Table 3) and other is the difference in catalyst acidity (Table 1). Considering the metal sulfide species surface exposure, the XPS results on sulfided catalysts show that support grafting with P (1.0–2.0 wt%) increased the surface exposure of the Mo species (Table 3). Thus, apparently, the enhancement of HDS activity by support modification with P (Fig. 5(a)) can be explained by improvement of the Mo surface exposure in the sulfided catalysts.

Taking into account that DBT adsorbs on a Mo and/or Ni sites, and may be even on the brim edge sites as shown by Besenbacher and co-workers [9,10], one might expect that the presence of P_2O_5 particles located on the support surface favor DBT adsorption on the metal sites, in particular on the brim sites. This may explain the superior HDS activity on the P-containing catalysts with respect to P-free sample. Another explanation for the improved activity of Cat-P1.0 sample could be the creation of a second hydrogenation pathway by spillover of hydrogen atoms from the metal sulfide particles to the DBT molecules that are adsorbed on acidic sites in the vicinity of the MoS_2 particles [53]. Indeed this sample exhibit the best acidic properties among the catalysts studied, as confirmed by IR study of adsorbed pyridine (Table 1). Interestingly, all P-containing samples exhibit a larger acidity than their P-free counterpart, as confirmed for oxide precursors by TPD-NH_3 (see SI) and for sulfide samples by DRIFT study of adsorbed pyridine (Fig. 1), which might to explain the larger activity of the former sample with respect to the latter. Unfortunately, for the P-containing samples, it was impossible to establish a more precise correlation between the catalyst acidity and their catalytic response. This is probably

Table 6
Activity and HYD/DDS selectivity ratio for the HDS of DBT in the presence of vary amount of carbazole [a].

Catalyst	$r_{DBT} \times 10^8$ ($mol_{DBT}\ g^{-1}_{cat.}\ s^{-1}$)				HYD/DDS selectvity's ratio at 30% conversion			
	N (ppm)				N (ppm)			
	0	50	100	180	0	50	100	180
Cat-P0.0	77	68	44	24	0.1	0.09	0.08	0.06
Cat-P1.0	123	111	84	64	0.28	0.26	0.22	0.15
Cat-P2.0	93	81	66	38	0.16	0.15	0.13	0.10
$NiMo/Al_2O_3$	79	72	59	47	0.19	0.17	0.14	0.08

[a] The reaction conditions were: $T = 320\,^{\circ}C$; $P = 55$ bar. The S and N concentrations were 50–180 ppm and 500 ppm, respectively; solvent: 90/10 wt% mixture of *n*-hexadecane/*p*-xylene.

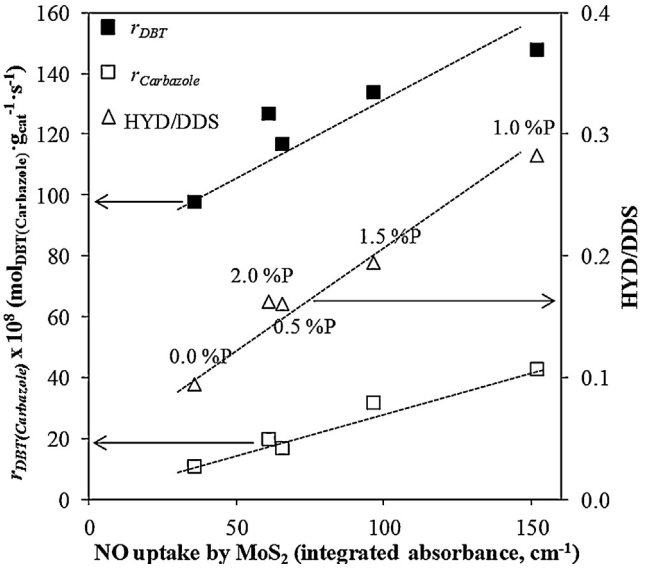

Fig. 9. Initial reaction rates of the individual reaction of DBT HDS and carbazole HDN, and HYD/DDS selectivities ratios (HDS of DBT) vs. NO uptake by MoS_2 determined from NO-FTIR spectroscopy.

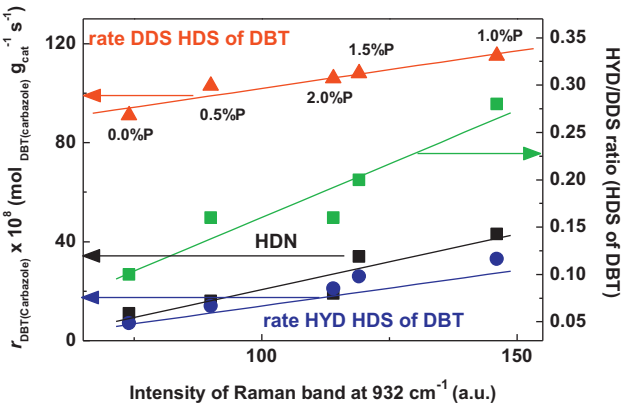

Fig. 10. Initial reaction rates for individual reactions of the HDS of DBT (rate via DDS and rate via HYD), HDN of carbazole and HYD/DDS selectivity's ratio (HDS of DBT) as a function of the intensity of Raman band at 932 cm^{-1} of oxide precursors.

because an increase in P loading from 0.5 to 2.0 wt% led to small differences in acidity of their oxide precursors and/or because of the pores plugging when a large amount of P was incorporated. Indeed, considering N_2 physisorption data (Table 1), the maximum in acidity and catalytic activity occurred at intermediate P level which can be explained considering its optimized textural properties because phosphate excess results in plugging of the pores.

In order to gain some insight between catalysts' structure and their corresponding catalytic activities, Fig. 9 shows the reaction rates for the HDS of DBT and the HDN of carbazole as well as the HYD/DDS ratio plotted against the calculated amount of NO uptake by MoS_2 determined from FTIR experiments. Both reaction rates and the HYD/DDS ratio increased almost linearly with the amount of MoS_2 present in the sulfided catalysts indicating a clear relationship between the amount of MoS_2 on the catalysts' surface and their catalytic activity in both HDS and HDN reactions. It is clear that this also enhanced the hydrogenating properties of the sulfided materials, as seen from the HYD/DDS ratios. It is well known that the amount of chemisorbed NO allows the estimation of the amount of coordinative unsaturated sites (CUS) which are responsible for the catalytic activity of HDS catalysts. Thus the observed increase in activity and in the hydrogenation properties of the P containing catalysts suggests that the introduction of P as a second promoter in the catalysts tested increased the amount of sulphur vacancies located on the corners of the active MoS_2 phase slabs, which participate in the creation of hydrogenation active sites [54–55]. The NO adsorption FTIR experiments also revealed the presence of both oxidized and sulfided Ni^{2+} species. Nevertheless, the presence of oxidized Ni species apparently did not affect negatively the activity of the catalysts. Similar observations have been made previously by different authors [13,15,56] in supported Co and CoMo catalysts. This effect was attributed to the participation of oxidized Co in the dissociative adsorption mechanism of H_2 and could be extended to oxidized Ni particles which might be in contact or not with the MoS_2 phase [57].

Another correlation between catalytic activity and catalysts' structure may be obtained from the characterization of the calcined materials. Fig. 10 shows initial reaction rates for individual reactions of the HDS of DBT (rate via DDS and rate via HYD), HDN of carbazole and HYD/DDS selectivity's ratio (HDS of DBT). As seen, there is a linear relationship between initial DDS and HYD rates of the DBT transformation, and the intensity of the Raman band assigned to the Mo=O terminal bonds. Furthermore, this linear relationship was also valid for the HYD/DDS selectivity's ratio (HDS of DBT) and initial reaction rate of the carbazole transformation. Interestingly, the HYD rate during HDS of DBT is close to that observed for HDN of carbazole. Considering our previous observation [13] and results reported by Atanasova et al. [25], this correlation can suggest the presence of irregular MoS_2 crystallites. The decrease in activity observed when P was increased to 2.0 wt% and the corresponding decrease in the Raman band intensity corresponding to M=O bonds may be explained by an increase in the degree of polymerization of Mo species via Mo—O—Mo bonds. An increase of polymerization of Mo species could have detrimental effect for the active phase formation during sulfidation as well as might to influence on the active phase dispersion, as deduced from XPS and HRTEM, respectively. However, more studies are needed in order to clarify this hypothesis.

4. Conclusions

The catalytic response of NiMo/P/HMS-Al sulfide catalysts in the individual and simultaneous HDS of dibenzothiophene and HDN of

carbozole reactions were investigated. It was found that support modification with optimized amount of P (1 wt%) decreased the inhibition of HDS reaction by carbazole. Regardless of the reaction studied, all P-containing catalysts showed higher activity than that to the P-free one. The catalyst modified with optimized amount of P exhibited the best HDS activity and a lowest inhibition factor during simultaneous HDS and HDN, which was close to that of a commercial $NiMo/Al_2O_3$ sulfide catalyst. This was linked with formation of irregular MoS_2 structures having high concentration of brim sites as well as to its high concentration of Brønsted and Lewis acid sites. On the contrary, the polymeric Mo—O—Mo particles were not precursors of the active phases formed upon sulfidation.

Acknowledgements

The authors are grateful to E. Flores, E. Aparicio, D. Dominguez, J.A. Díaz, F. Ruiz and I. Gradilla for their technical assistances and CONACYT projects 152012, 155388 and 117373 for the financial supports.

Appendix A. Supplementary data

Supplementary data associated with this article can be found, in the online version, at http://dx.doi.org/10.1016/j.apcatb.2015.07.013

References

[1] (a) T.C. Ho, J. Catal. 219 (2003) 442–451;
(b) T.C. Ho, Catal. Today 98 (2004) 3–18;
(c) T.C. Ho, Chem. Eng. Commun. 193 (4) (2006) 460–477.
[2] T.C. Ho, D. Nguyen, J. Catal. 222 (2004) 450–460.
[3] T.C. Ho, L. Qiao, J. Catal. 269 (2010) 291–301.
[4] H. Kraus, R. Prins, J. Catal. 170 (1997) 20–28.
[5] M. Nagai, T. Sato, A. Aiba, J. Catal. 97 (1986) 52–58.
[6] J. Hrabar, O.Y. Hein, J.A. Gutiérrez Lercher, J. Catal. 281 (2011) 325–338.
[7] A. Infantes-Molina, J.A. Cecilia, B. Pawelec, J.L.G. Fierro, E. Rodríguez-Castellón, A. Jimenez-López, Appl. Catal. A: Gen. 390 (2010) 253–263.
[8] H. Topsøe, B. Hinnemann, J.K. Nørskov, J.V. Lauritsen, F. Besenbacher, P.L. Hansen, G. Hytoft, R.G. Egeberg, K.G. Knudsen, Catal. Today 107–108 (2005) 12–22.
[9] J.V. Lauritsen, M.V. Bollinger, E. Lægsgaard, K.W. Jacobsen, J.K. Nørskov, B.S. Clausen, H. Topsøe, F. Besenbacher, J. Catal. 221 (2004) 510–522.
[10] J.V. Lauritsen, M. Nyberg, J.K. Nørskov, B.S. Clausen, H. Topsøe, E. Lægsgaard, F. Besenbacher, J. Catal. 224 (2004) 94–106.
[11] H. Topsøe, B.S. Clausen, F.E. Massoth, in: J.R. Anderson, M. Boudart (Eds.), Catalysts: Science and Technology, vol. 11, Springer, Berlin, 1996, pp. 111–191.
[12] M. Breysse, P. Afanasiev, C.H. Geantet, M. Vrinat, Catal. Today 86 (2003) 5.
[13] T.A. Zepeda, B. Pawelec, J.L.G. Fierro, A. Montesinos, A. Olivas, S. Fuentes, T. Halachev, Microporous Mesoporous Mater. 111 (2008) 493–506.
[14] R. Iwamoto, J. Grimblot, Adv. Catal. 44 (1999) 417–503.
[15] B. Pawelec, J.L.G. Fierro, A. Montesinos, T.A. Zepeda, Appl. Catal. B: Environ. 80 (2008) 1–14.
[16] R. Huirache-Acuña, B. Pawelec, E. Rivera-Muñoz, R. Nava, J. Espino, J.L.G. Fierro, Appl. Catal. B: Environ. 92 (2009) 168–184.
[17] M.A. Guzmán, R. Huirache-Acuña, C.V. Loricera, J.R. Hernández, J.N. Díaz de León, J.A. de los Reyes, B. Pawelec, Fuel 103 (2013) 321–333.
[18] R. Nava, A. Infantes-Molina, P. Castaño, R. Guil-López, B. Pawelec, Fuel 90 (2011) 2726–2737.
[19] S. Sigurdson, V. Sundaramurthy, A.K. Dalai, J. Adjaye, J. Mol. Catal. A: Chem. 291 (2008) 30–37.
[20] J.M. Lewis, R.A. Kydd, P.M. Boorman, P.H. Van Rhyn, Appl. Catal. A: Gen. 84 (1992) 103–121.
[21] C.W. Fitz, H.F. Rase, Ind. Eng. Chem. Prod. Res. Dev. 22 (1983) 40–44.
[22] M. Sun, D. Nicosia, R. Prins, Catal. Today 86 (2003) 173–189.
[23] S. Damyanova, A. Spojakina, Z. Vít, Collect. Czech. Chem. Commun. 57 (1992) 1033–1042.
[24] J.L.G. Fierro, A. López Agudo, N. Esquivel, R. López Cordero, Appl. Catal. 48 (1989) 353–363.
[25] P. Atanasova, T. Halachev, J. Uchytil, M. Kraus, Appl. Catal. A: Gen. 38 (1988) 235–240.
[26] R. López Cordero, L. López Guerra, J.L.G. Fierro, A. López Agudo, J. Catal. 126 (1990) 8–12.
[27] A. Spojakina, S. Damyanova, L. Petrov, Z. Vit, Appl. Catal. 56 (1989) 163–176.
[28] S. Eijsbouts, J.N.M. van Gestel, J.A.R. van Veen, V.H.J. de Beer, R. Prins, J. Catal. 131 (1991) 412–432.
[29] J.A.R. van Veen, H.A. Colijn, P.A.J.M. Hendriks, A.J. van Welsenes, Fuel Process. Technol. 35 (1993) 137–157.
[30] P.T. Tanev, T.J. Pinnavaia, Science 267 (1995) 865–867.
[31] S. Gontier, A. Tuel, Zeolites 15 (1995) 601–610.
[32] C.T. Kresge, M.E. Leonowich, W.J. Roth, J.C. Vartuli, J.S. Beck, Nature 359 (1992) 710–712.
[33] S. Kawi, S.C. Shen, P.L. Chew, J. Mater. Chem. 12 (2002) 1582–1586.
[34] V. La Parola, G. Deganello, C.R. Tewell, A.M. Venezia, Appl. Catal. A: Gen. 235 (2002) 171–180.
[35] C.A. Emeis, J. Catal. 141 (1993) 347–354.
[36] B. Chakraborty, B. Viswanathan, Catal. Today 49 (1999) 253–260.
[37] G. Busca, Catal. Today 41 (1–3) (1998) 191–206.
[38] N.Y. Topsøe, H. Topsøe, J. Catal. 84 (1983) 386–401.
[39] J.L.G. Fierro (Ed.), Spectroscopic characterization of heterogeneous catalysts. Part: B: Chemisorption of probe molecules, Stud. Surf. Sci. Catal., Vol. 57, Elsevier, Amsterdam, 1990, p. 126.
[40] X. Wang, U.S. Ozkan, J. Catal. 227 (2004) 492–501.
[41] A.Y. Bunch, X. Wang, U.S. Ozkan, Appl. Catal. A: Gen. 346 (2008) 96–103.
[42] A.D. Gandubert, E. Krebs, C. Legens, D. Costa, D. Guillaume, P. Raybaud, Catal. Today 130 (2008) 149–159.
[43] B. Guichard, M. Roy-Auberger, E. Devers, C. Legens, P. Raybaud, Catal. Today 130 (2008) 97–108.
[44] M. Egorova, R. Prins, J. Catal. 221 (2004) 11–19.
[45] M. Vrinat, Appl. Catal. 6 (1983) 137–158.
[46] H. Farag, D.D. Whitehurst, K. Sakanishi, I. Mochida, Catal. Today 50 (1999) 49–56.
[47] K. Gishti, A. Iannibello, S. Marengo, G. Morelli, P. Tittarelli, Appl. Catal. 12 (1984) 381–393.
[48] A. Ishihara, T. Itoh, T. Hino, M. Nomura, P. Qi, T. Kabe, J. Catal. 140 (1993) 184–189.
[49] A. Guevara, R. Bacaud, M. Vrinat, Appl. Catal. A: Gen. 253 (2003) 515–526.
[50] G.C. Laredo, J.A. de los Reyes, J.L. Cano, J.J. Castillo, Appl. Catal. A: Gen. 207 (2001) 103–112.
[51] W.C. Cheng, N.P. Luthra, J. Catal. 109 (1988) 163–169.
[52] Y. Teng, A. Wang, X. Li, J. Xie, Y. Wang, Y. Hu, J. Catal. 266 (2009) 369–379.
[53] (a) S.D. Lin, M.A. Vannice, J. Catal. 143 (1993) 539–553;
(b) S.D. Lin, M.A. Vannice, J. Catal. 143 (1993) 554–562;
(c) S.D. Lin, M.A. Vannice, J. Catal. 143 (1993) 563–572.
[54] J. Ch. Papadopoulou, H.K. Vakros, G.A. Matralis, J. Voyiatzis Ch Kordulis, Colloid Interface Sci. 274 (2004) 159–166.
[55] S. Cristol, J.F. Paul, E. Payen, D. Bougeard, F. Hutschka, S. Clemendot, J. Catal. 224 (2004) 138–147.
[56] A.M. Venezia, R. Murania, G. Pantaleo, G. Deganello, J. Mol. Catal A: Chem. 271 (2007) 238–245.
[57] R.I. Declerck-Grimes, P. Canesson, R.M. Friedman, J.J. Fripiat, J. Phys. Chem. 82 (1978) 889–893.